ACS APPLIED MATERIALS & INTERFACES

www.acsami.org Research Article

Wearable System Integrating Dual Piezoresistive and Photoplethysmography Sensors for Simultaneous Pulse Wave Monitoring

Borzooye Jafarizadeh, Azmal Huda Chowdhury, Md Shariful Islam Sozal, Zhe Cheng, Nezih Pala, and Chunlei Wang*

Cite This: *ACS Appl. Mater. Interfaces* 2024, 16, 65402−65413 Read Online

ACCESS | Metrics & More | Article Recommendations | Supporting Information

Downloaded via FLORIDA INTL UNIV on April 9, 2026 at 20:08:58 (UTC).
See https://pubs.acs.org/sharingguidelines for options on how to legitimately share published articles.

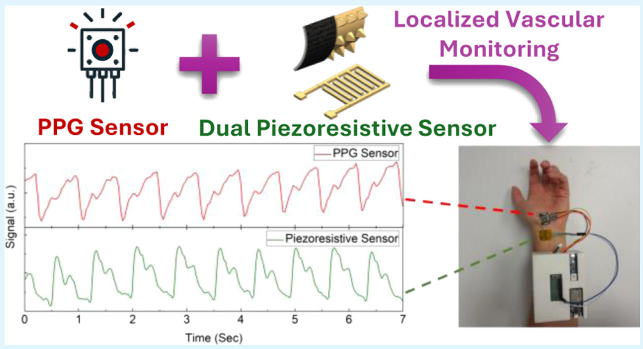

ABSTRACT: Wearable, flexible piezoresistive pressure sensors have garnered substantial interest due to their diverse applications in fields such as electronic skin, robotic limbs, and cardiovascular monitoring. Among these applications, arterial full pulse waveform monitoring stands out as a critical area of research. The emergence of piezoresistive pressure sensors as a prominent tool for capturing pulse waveforms has led to extensive investigations. However, the lack of a linear response while achieving high sensitivity, limited compactness of signal collection systems, and scaling issues are a few potential causes of the gap between research advances and technology market readiness. Here, we present a scalable dual piezoresistive sensor that uses two complementary resistance-changing mechanisms to balance the trade-off between linear response and high sensitivity. This synergic design enables excellent sensitivity of 8.4 kPa^{-1} and near linear pressure response. It boasts a fast response time of 95/145 ms for loading and unloading at a pressure of 10.1 kPa. The durability tests, encompassing nearly 5000 two-stage compression cycles, validate the reliable performance of the sensor, even after prolonged use. Leveraging these performance metrics, we developed a high-resolution and compact signal collection device capable of accurately detecting the three distinct peaks associated with the full pulse waveform, including the systolic and reflected diastolic peaks. Moreover, the signal acquisition system incorporates a photoplethysmography sensor, which, when paired with the dual piezoresistive sensor, offers new insights into localized vascular health monitoring. The unique feature of our approach is its ability to perform localized vascular monitoring using multiple sensors placed on different veins. The simultaneous detection of forward- and backward-going pulse waves at the body extremities allows for a comprehensive evaluation of localized vascular health, which is not achievable with a single sensor. Finally, the comparison of wrist pulse waveforms between the compact signal collection device and a standard sourcemeter (such as the Keithley 2460) confirmed that the wearable sensing system is on par with conventional sourcemeters in terms of capturing the typical details of the full pulse waveform (i.e., systolic peak, dicrotic notch, and diastolic peak). This validation underscores the reliability and effectiveness of the developed wearable sensing system for practical and continuous pulse waveform monitoring.

KEYWORDS: *piezoresistive pressure sensor, wearable, arterial pulse, pulse waveform, signal acquisition, sensitivity*

1. INTRODUCTION

Wearable technology's promise of convenient round-the-clock cardiovascular health monitoring has prompted extensive research on high performance sensors. One potential category of cardiovascular health monitoring devices is flexible pressure sensors that can detect both human motion and some weak physiological signals. Efforts have been focused on developing sensors that can detect minute pressure variations on the skin and convert them into detectable electrical signals. These efforts have yielded significant improvements in various areas, including cardiovascular health monitoring,[1−3] robotics, and[4,5] human−robot hybridization.[6] Additionally, with the introduction of new high-capacity batteries,[7] these sensors can now be deployed in form of worn accessories for extended periods of time. The pressure ranges in which a wearable sensor operates vary depending on the requirements of the application. Particularly, they are divided into three categories: low

Received: October 14, 2024
Revised: November 1, 2024
Accepted: November 5, 2024
Published: November 12, 2024

pressure (<1 Pa), medium pressure (1−20 kPa), and finally, high pressure (20−100 kPa).[2,3] Research in recent years has largely focused on pressure sensors operating in low-to-medium pressure regimes because of the applications in human health and fitness monitoring, including blood pressure and pulse waveform measurement. Based on the working mechanism, pressure sensors can be divided into four types including piezoresistive,[5,8,9] capacitive,[6,10] piezoelectric,[11,12] and triboelectric.[13,14] Due to their quick response times and straightforward signal acquisition, piezoresistive sensors have gained popularity as the practical choice for flexible pressure sensors in wearable cardiovascular health monitoring.

To create highly sensitive piezoresistive pressure sensors, researchers have proposed various architectures and sensing materials.[15−17] The literature has documented two mechanisms of resistance change in piezoresistive sensors. The first mechanism can be simply summarized when tiny features on the surface undergo deformation; it leads to a change in the contact area between conductive layers, resulting in a signal. Sensors in this category typically employ micropyramids, microdomes, micropillars, microcones, or other microfeatures.[15,16,18−20] The second mechanism employs a conductive porous material, such as a MXene porous layer, for signal generation.[18,19] When a sensor utilizing this mechanism is deformed, the porous material's electrical resistance changes due to the interplay of tunneling effects within its porous structure. Despite the successful development of piezoresistive pressure sensors for acquiring the full pulse waveform from peripheral arteries, it remains challenging to transition from the laboratory development stage to clinical trials and the market. The gap between successful development of piezoresistive pressure sensors and their practical adoption may arise from several factors: testing schemes that do not accurately mirror real-world wearable functionality, complexity and size of signal acquisition devices, and challenges related to scaling.

In terms of reliable wearable functioning, piezoresistive pressure sensors capable of detecting human pulse waves in a benchtop configuration have been developed;[21−23] nevertheless, accomplishing the same task by a compact wearable signal collection device is still difficult. Primarily because the signal level and signal-to-noise ratio are typically low (<10 μA) (Figure S1[18,24−31]); therefore, complex and bulky signal acquisition devices are typically used to filter out the noise. Moreover, by convention, the response time is measured as the duration it takes for the sensor's output to stabilize when a constant pressure is applied.[5,6,32,33] To offer a more precise response time for piezoresistive pressure sensors, it is crucial to address a limitation inherent in the conventional testing method. Specifically, as the applied pressure increases, the reaction time also extends. Therefore, it is essential to acknowledge that the response time of piezoresistive sensors should not be considered an independent variable in relation to the applied pressure. Similarly, the durability of such sensors is often tested in an unknown applied pressure, despite the fact that the sensor's degradation is influenced by the intensity of the load.[18−20,22,24,25,27,28,34−] Thus, in order to ensure reliable operation of piezoresistive pressure sensors (e.g., in peripheral pulse waveform monitoring), enhanced testing schemes are required to overcome the above-mentioned shortcomings and improve practical operation of wearable piezoresistive pressure sensors.

Therefore, to create a piezoresistive sensor suitable for pulse monitoring, it is essential to implement solutions that address the aforementioned limitations, ensuring robust wearability and scalability. In this study, aimed at enhancing the technology readiness level, we initially conducted finite element analysis (FEA) to comprehend the relationship between the output current and pressure for sensors crafted from materials of varying conductivities. To address the limitations of current piezoresistive pressure sensors, we present a novel dual piezoresistive sensor that synergistically employs two simultaneous resistance-changing mechanisms, which uniquely balance the trade-off between high sensitivity and linear response—a key challenge in existing designs. Subsequently, a specialized testing protocol and programmable hardware are developed for evaluating the piezoresistive pressure sensors, ensuring that they meet the functional requirements for wearable pulse waveform detection. Moreover, to solve the problem of bulky signal acquisition systems, we developed a fully wearable and compact signal collection device capable of simultaneously collecting signals from multiple sensors, enabling reliable and comprehensive pulse detection. This integrated system not only enhances portability but also offers the potential to capture complementary data such as volumetric vein size changes via PPG and a fraction of blood pressure via the piezoresistive pressure sensor. By combining these signals, the system may enable the measurement of clinically relevant parameters, such as pulse wave velocity (PWV), which is important for assessing arterial stiffness and cardiovascular health.[38] While our system does not report PWV values currently, it provides the necessary raw data from a noninvasive technique for its calculation, offering a pathway to future clinical applications.

2. EXPERIMENTAL DETAILS

2.1. Materials. Polydimethylsiloxane (PDMS), a silicone-based elastomer with two cross-linkable components (Sylgard 184), was purchased from Thermo Fisher Scientific. DWK Life Sciences Silicone Grease Tube and Carbon Black were procured from Thermo Fisher Scientific. Whatman Qualitative Filter Paper: grade 4 (pore size 25 μm) was procured from Sigma-Aldrich. Kapton tape was acquired from 3M (USA). The 100 nm Si_3N_4 wafer was purchased from SPI supplies (USA). And finally, screen-printed interdigitated electrodes (IDEs) (this is a specific electrode layout consisting of two sets of closely spaced, comb-like fingers that interlock, resembling the teeth of a zipper; refer to Figure S3 for dimensions) were purchased from Ohmite (USA). All chemicals were used without additional treatment, and deionized water was used for all the experiments.

2.2. Preparation of Micropyramid Component of the Dual Piezoresistive Sensor. The silicon mold was created using a laser writer (HIEDELBERG μPG101) to generate a mask, followed by a series of processes, including photolithography, dry etching, and wet etching (depicted in Figure S2). The silicon wafer was patterned using standard photolithography techniques, and reactive ion etching (dry etching) was utilized to selectively remove Si_3N_4 according to the design. The remaining Si_3N_4 acted as a protective mask during the wet etching process, which entailed immersing the wafer in a KOH bath at 80 °C for about 4 h. The final silicon mold is reusable. To create the micropyramid layer, the silicon mold surface is first treated by placing it in a vacuum desiccator alongside 1 mL of 1*H*,1*H*,2*H*,2*H*-perfluorooctyl trichlorosilane for 1 h. Subsequently, 10 mL of uncured PDMS is prepared in a 1:10 ratio (cross-linker to base polymer) by vigorous mixing for 5 min. This mixture is degassed in a vacuum desiccator for 30 min. The mixture is then applied to the silicon mold and maintained at 20 °C until the PDMS is fully cured, which takes approximately 72 h. In the final step, the micropatterned PDMS is carefully detached, surface treated according to the process explained by Kim et al.[4] and a 200 nm layer of gold is sputtered onto its surface using physical vapor deposition.

https://doi.org/10.1021/acsami.4c17710
ACS Appl. Mater. Interfaces 2024, 16, 65402−65413

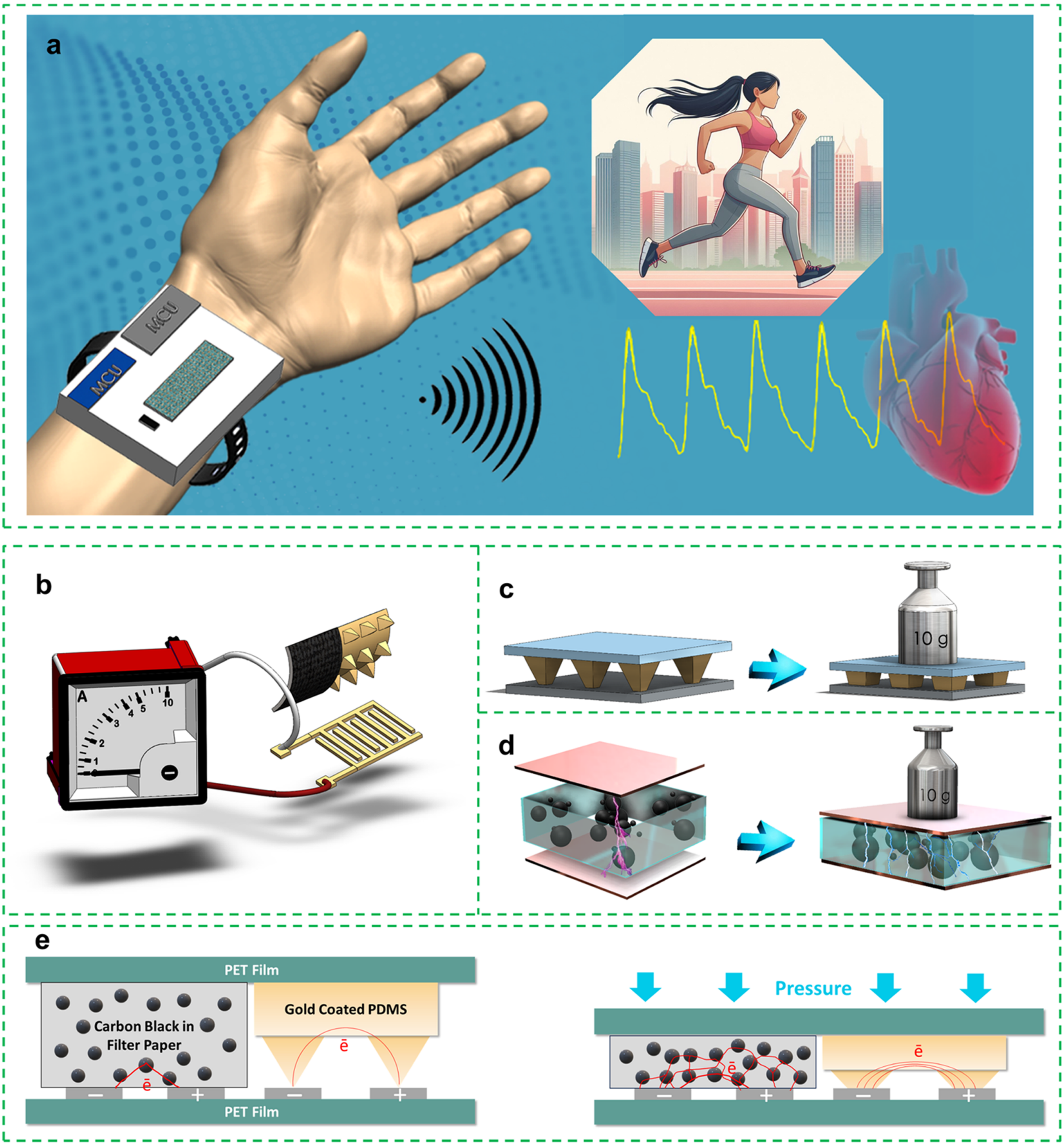

Figure 1. (a) Schematic illustrating the pressure sensing system. (b) Illustrative electrical circuit demonstrating the configurative placement of both components of the dual piezoresistive sensor. Schematic illustrating how application of pressure leads to increased electron transport in (c) a piezoresistive sensor employing surface asperity, (d) a piezoresistive sensor utilizing conductive porous material, and (e) the dual piezoresistive pressure sensor that combines both aforementioned mechanisms into one sensor.

2.3. Preparation of Porous Component of the Dual Piezoresistive Sensor. The conductive grease was prepared by mixing carbon black (20 wt %) with silicon grease in a mixing bowl until the carbon black is evenly distributed throughout the grease with uniform black color. The mixture was transferred to an airtight container for storage. This portion of the sensor (Figure 1d) is fabricated by coating the filter paper with 0.1 mL of conductive grease. Then the filter paper is cut to a size of 1 × 1 cm^2 and put aside. The conductive coating had thickness of about 100 μm, which was then dried on a hot plate at 100 °C for 24 h. Later, it was stored in a vacuum desiccator to keep the material dry before sensor assembly.

2.4. Dual Piezoresistive Sensor Assembly. The micropyramid component, along with the conductive porous component, is positioned side-by-side facing the IDE. Subsequently, external wires are soldered to the terminals of the IDE (Figure 1b). The final step involves encapsulating the assembly with the Kapton tape to create a flexible pressure sensor.

https://doi.org/10.1021/acsami.4c17710
ACS Appl. Mater. Interfaces 2024, 16, 65402−65413

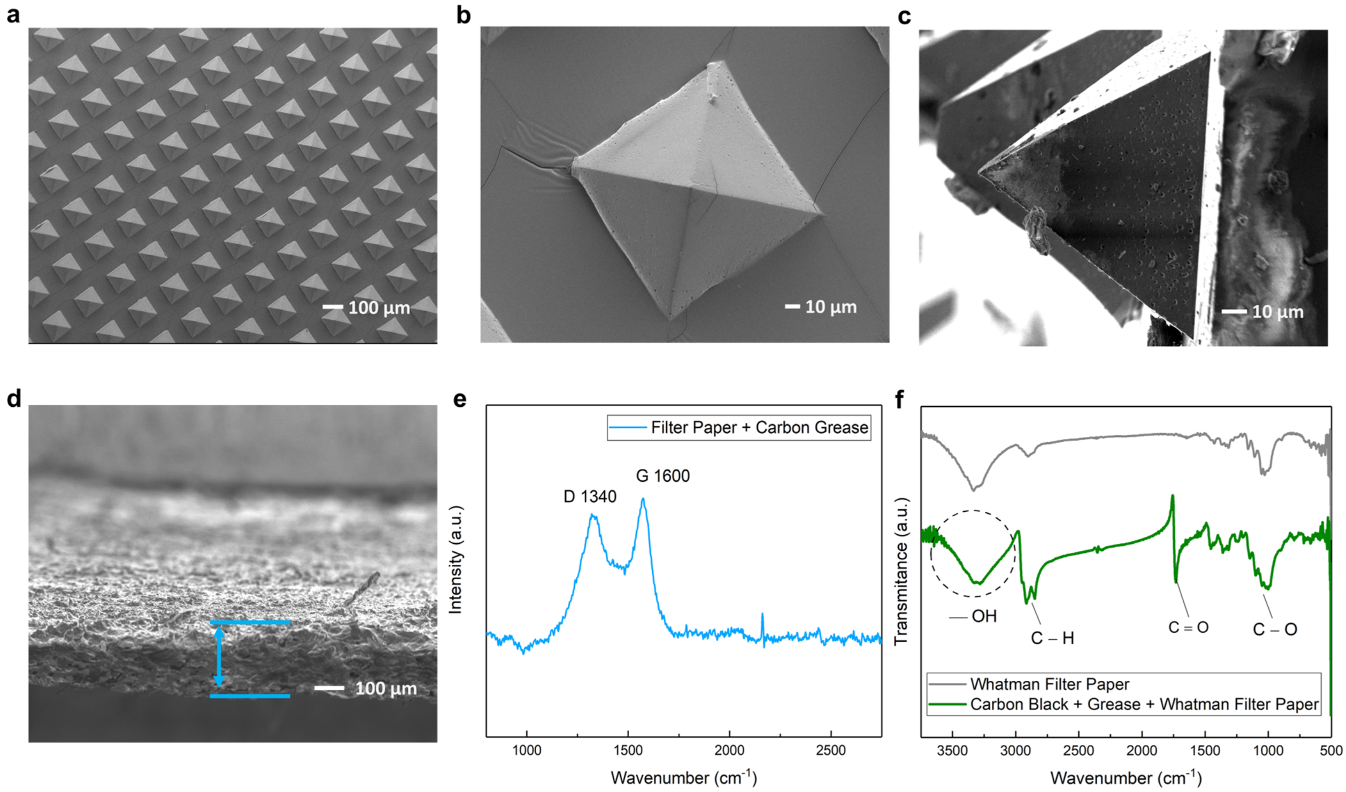

Figure 2. (a−c) SEM images from both top view and cross-section view depicting the micropyramid layer. (d) SEM image displaying the porous piezoresistive component cross-section. (e) Raman spectroscopy of the synthesized porous piezoresistive sensing material. (f) FTIR spectra of both the synthesized porous piezoresistive sensing material and the filter paper substrate without coating.

2.5. Characterization. Surface morphologies and cross-sections of the components were observed with scanning electron microscopy (SEM, JSM-F100, JEOL, Japan). The Fourier transform infrared spectroscopy was conducted to confirm the surface functional groups (FT/IR-4100, Jacso, Japan). Raman Spectroscopy was utilized to confirm the chemical and functional groups (MultiView 2000TS system with built-in Raman spectroscopy, Nanonics Imaging Ltd., Israel). The pressure sensors were calibrated against a Force Gauge (Mark-10, Johnson Scale Co).

2.6. Signal Acquisition. The benchtop signal readout from the sensor was carried out using sourcemeter (Keithley 2460, Keithley Instruments). The wearable data acquisition was realized by compact development boards ESP32-S and Arduino Nano BLE 33 in conjunction with the ADS1256 (24-bit external analogue to digital convertor). The power supply for this system was a 1000 mAh 7.2 V LiPo battery, and its output was stepped down to 5.5 V using LM2596 DC to DC high efficiency voltage regulator.

3. RESULTS AND DISCUSSION

3.1. Material Characterization. Figure 1a illustrates the suggested placement for the wrist-worn dual piezoresistive pressure sensor and signal acquisition system. The compact system allows for continuous and wearable pulse waveform recording. Unlike previous studies using expensive, bulky sourcemeters,[12,13,15,23] this design integrates a wearable signal acquisition device proficient in capturing pulse waveforms with sufficient details to discern the three characteristic peaks of pulse waveforms. The system is designed to be able to acquire the full pulse waveform, transmit the data in real-time to a server, and post process the data (e.g., feature extraction) as needed.

The dual piezoresistive sensor comprises two complementary components, offering nearly linear sensitivity across an extensive pressure range. The simplified electrical circuit models the components as two variable resistors facing an IDE configuration with a constant voltage difference. External pressure, like a pulse wave, induces variations in electrical current, which are detected by a device akin to a sourcemeter (Figure 1b). The micropyramid component (Figure 1c), which can function as a standalone piezoresistive sensor, provides high sensitivity in the low-pressure regime (<1 kPa). In contrast, the conductive filter paper component (Figure 1d) ensures both higher pressure sensitivity and linearity in the 1−20 kPa range. This is ideal for pulse measurements at elevated pressures.[3] Since both components can independently operate as piezoresistive sensors, the device is referred to as a dual piezoresistive pressure sensor. The working mechanism of this sensor is illustrated in Figure 1e, which provides a side view of the internal components. When pressure is applied, it induces compressive strain in the porous filter paper component, bringing the carbon black particles closer together. This increases the number of available tunneling paths for electron movement, thereby reducing the sensor's resistivity. Similarly, as the micropyramid component is compressed, its contact area with the individual teeth of the interdigitated electrode (IDE) increases, allowing more electron pathways to form between the teeth. As a result, an increase in the passing current is observed during sensor operation when subjected to pressure.[3]

Scanning electron microscopy (SEM) is utilized to examine individual components of the dual piezoresistive sensor (Figure 2a−d). The array of micropyramids provides surface asperities with dimensions of 100 μm at the base and approximately 70 μm in height. The deposition of a gold

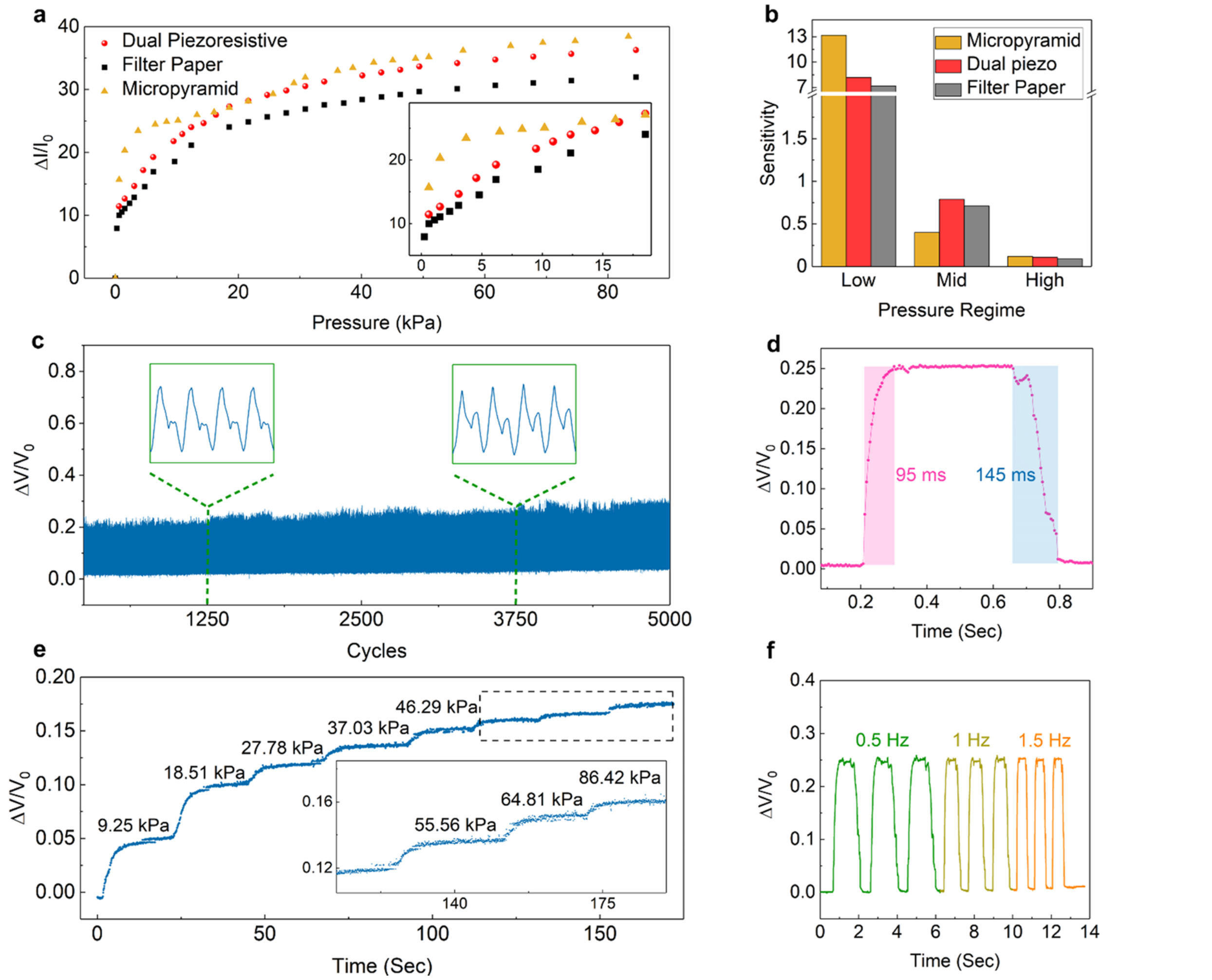

Figure 3. Sensing performance of the dual piezoresistive pressure sensor. (a) Pressure response plot of dual piezoresistive pressure sensor and sensors made from individual micropyramid based and conductive filter paper-based pressure sensors. (b) Chart summarizing the sensitivity of the pressure sensors for low (<1 kPa), mid (1−20 kPa), and high (20−90 kPa) pressure regimes. (c) Cyclic stability test of the dual piezoresistive sensor for synthetic waveforms comprising of two peaks. (d) Response and recovery time of the dual piezoresistive under 10.1 kPa. (e) Response of the pressure sensor under stepwise loading. (f) Response of the pressure sensor under different frequencies (i.e., 0.5, 1, and 1.5 Hz) of pulse wave.

coating via sputtering on this component endows it with heightened conductivity (~10^5 S/m), consequently yielding substantial changes in current when subjected to a constant potential across the terminals of the interdigitated electrode (IDE) (Figure S3). The SEM images of the micropyramid component (Figure 2a−c) reveal sharply defined features at their tips, indicating the successful completion of the wet etching process as the features exhibit no signs of tapering. While one micropyramid in Figure 2c shows a tip defect, this damage occurred due to a mechanical accident post-fabrication, rather than an issue with the etching process itself. As all micropyramids are etched simultaneously, incomplete etching would result in defects across all tips, which is clearly not the case here, as demonstrated by the intact sharp tip of the adjacent pyramid.[17]

Figures 2d and S6 shows the SEM cross-sectional image of the porous carbon black-based conductive component. This porous conductive material is incorporated to enhance the performance of the dual piezoresistive pressure sensor. By providing multiple conductive pathways under compression, the component is designed to support more consistent sensor behavior at higher compressive strains. Additionally, the fabrication of this sensor is suited to be scaled. Costly and time-intensive procedures, such as lithography, deposition, etching, and cleanroom protocols, are exclusively required to produce the micropyramid mold. The mold's reusability to fabricate the micropyramid component along with the uncomplicated process to realize the porous component contribute to the scalability of dual piezoresistive sensor manufacturing.

The Raman spectrum of the fabricated conductive grease in the range of 1000−2750 cm^{-1} is presented in Figure 2e. The spectrum mainly consists of two relatively broad bands. One G (graphite) band at 1600 cm^{-1} ascribed to sp^2 hybridized and another D (defect or disorder) around 1340 cm^{-1} associated with sp^3 hybridized carbons.[39] The Fourier Transform Infrared (FTIR) spectroscopy of the fabricated conductive grease (Figure 2f) reveals several characteristic peaks that differ from the spectra of the substrate (Whatman filter paper) depicted in Figure 2c. The broad band at 3400 cm^{-1} corresponds to O−H stretching vibrations, indicative of hydroxyl groups or water present in both samples. The more intense O−H stretching band observed in the carbon grease spectrum suggests a higher degree of water absorption, which can be attributed to the

https://doi.org/10.1021/acsami.4c17710
ACS Appl. Mater. Interfaces 2024, 16, 65402−65413

porous structure of the carbon black. In the 2800−3000 cm^{-1} region, distinct peaks associated with C−H stretching vibrations are present only in the carbon grease sample, indicating the presence of aliphatic hydrocarbons likely stemming from oils or lipids used in the grease formulation. These peaks are absent in the Whatman filter paper spectrum, reflecting the different chemical composition between the two materials. Additionally, the peak observed at ∼1630 cm^{-1} in the carbon grease spectrum, which is absent in the filter paper, is ascribed to C═C stretching vibrations. This indicates the presence of unsaturated hydrocarbons or aromatic components in the carbon grease paste. Moreover, a prominent peak around 1750 cm^{-1} is noted in the carbon grease spectrum, corresponding to C═O stretching vibrations, which suggests the presence of carbonyl groups such as esters. These esters are likely derived from the synthetic or natural oils used in the formulation of the grease.[40] The Raman spectrum is consistent with the FTIR observations, confirming the presence of carbon-based materials. The prominent D band at ∼1340 cm^{-1} and G band at ∼1600 cm^{-1} in the Raman spectrum are characteristics of disordered and graphitic carbon structures, respectively.

3.2. Finite Element Analysis. High signal strength is crucial for piezoresistive sensors to facilitate easy signal acquisition. Finite element analysis (FEA) has revealed that the conductivity value of the sensing material significantly affects the signal strength. The FEA model comprises a flexible layer with cone-shaped elastic surfaces at +1 V and a grounded layer without surface asperities (see Figure S4 in Supporting Information). Simulation results indicate that conductivity values below 1 S/m result in signal output levels below 100 nA, which can cause issues with signal acquisition due to a low signal-to-noise ratio. To achieve a stronger signal (larger ΔI) and higher sensitivity, the sensing material must possess high conductivity, as demonstrated in Figure S4b. Therefore, the incorporation of high conductivity fillers (such as carbon black) and coatings (such as gold) aligns with the goal of achieving excellent sensor materials. Elastic deformation from locally induced stresses increases layer contact area, affecting the sensor's overall electrical resistance. According to Figure S4c, decreasing conductivity from 10^3 to 1 S/m reduces sensitivity from 1 to 0.66 kPa^{-1}. High conductivity coatings (10^5 S/m), within the range of a 200 nm gold coating, yield milliamp-range current outputs, enabling convenient wearable signal acquisition using readily available development boards (e.g., ESP32 or Arduino). Furthermore, the high signal-to-noise ratio (SNR) signals achieved from such portable/wearable systems enable future deployment of machine learning models for real-time data processing tasks like feature extraction.

3.3. Performance Characteristics of the Dual Piezoresistive Sensor. When it comes to obtaining weak physiological signals from body peripherals, such as the heart's pulse waveform (from wrist, foot, etc.), the sensor's sensitivity is probably the most important sensor characteristic. Generally, the sensitivity (S) is defined as $S = \partial\,(\Delta I/I_0)/\partial P$, where I_0 is the initial current of the device without applied pressure and ΔI stands for current change under pressure P.

Initially, the sensing performance of the dual piezoresistive sensor along with two individual sensors out of the comprising components, i.e., one sensor based on a micropyramid as the sensing layer and another sensor based on conductive porous filter paper as the sensing layer. The results presented in Figure 3a demonstrate that the micropyramid exhibits very high initial sensitivity of 13 kPa^{-1} in the low-pressure regime (0−1 kPa) followed by a decrease in sensitivity to 0.41 kPa^{-1} in the midrange (1−20 kPa). This sharp decrease in sensitivity, akin to a stepwise behavior, as also observed by Kim et al.,[4] is attributed to the saturation of the contact area between the pyramidal structure and the IDE. In this study, to mitigate this stepwise behavior and enhance the linearity of the response, the micropyramid is paired with another piezoresistive sensing component, namely synthesized conductive porous filter paper, as shown in Figure 1b. In Figure 3b, the dual piezoresistive sensor demonstrates a sensitivity of 8.2 kPa^{-1} in the low range (<1 kPa), which remains notably high when compared to recent works with similar structures (Table S1). In the midrange (1−20 kPa), it exhibits a sensitivity of 0.79 kPa^{-1}, outperforming both standalone components. Specifically, a sensor made with only porous conductive material (carbon black + grease + filter paper) would have a sensitivity of 0.7 kPa^{-1}, while a sensor with micropyramid features would have a sensitivity of 0.4 kPa^{-1}. Thus, the dual piezoresistive pressure sensor achieves a superior performance in this range. However, in the extended high-pressure range (20−90 kPa), the sensitivities of the three sensors become similar, with values of 0.12 kPa^{-1} for the micropyramid, 0.11 kPa^{-1} for the dual piezoresistive sensor, and 0.09 kPa^{-1} for the filter paper sensor. These small differences in sensitivity at higher pressures do not translate to significant performance differences, as their practical sensitivity levels in this range are nearly the same.

It is important to note that while the sensitivity has been tested up to 90 kPa for completeness, the critical pressure range for pulse waveform monitoring is 1−20 kPa. In this key range, the dual piezoresistive sensor demonstrates higher sensitivity and superior linearity compared with the micropyramid and filter paper sensors. This is crucial for accurately capturing the detailed features of pulse waveforms, such as systolic and diastolic peaks, which are essential for cardiovascular monitoring. Sensors operating in the 40−100 kPa range may have applications in areas such as tactile sensing, industrial pressure monitoring, and robotics, where higher pressures are common. This configuration of the dual piezoresistive sensor not only enhances sensitivity characteristics but also improves response linearity, crucial factors for practical applications such as pulse waveform detection. Furthermore, these values exceed the sensitivities of piezoresistive sensors that have been introduced to acquire pulse waveforms from peripherals[18−20,25,27,28,36,37] illustrating the sensor's ability to maintain adequate sensitivity within pressure range relevant to blood pressure measurements (normal blood pressure is 0−16 kPa (120 mmHg)). Notably, the side-by-side configuration of the two piezoresistive components atop the IDE prevents the saturation of the IDE by the pyramidal structure and allocates half of the IDE to the mechanism responsible for enhancing the linearity of the pressure sensor. Figure 3c showcases the excellent repeatability and stability of the dual piezoresistive sensor. The stability and durability of the dual piezoresistive sensor are confirmed through approximately 5000 two-wave compression cycles. The custom-made testbed[41] at each cycle initiates compression at 12 kPa, releases to 50%, compresses to 70%, and finally releases to 0%. This comprehensive test assesses repeatability and examines possible hysteresis behavior over a comparably complex waveform at 5000 cycles of operation. The gradual increase in output over time may be attributed to several

https://doi.org/10.1021/acsami.4c17710
ACS Appl. Mater. Interfaces 2024, 16, 65402−65413

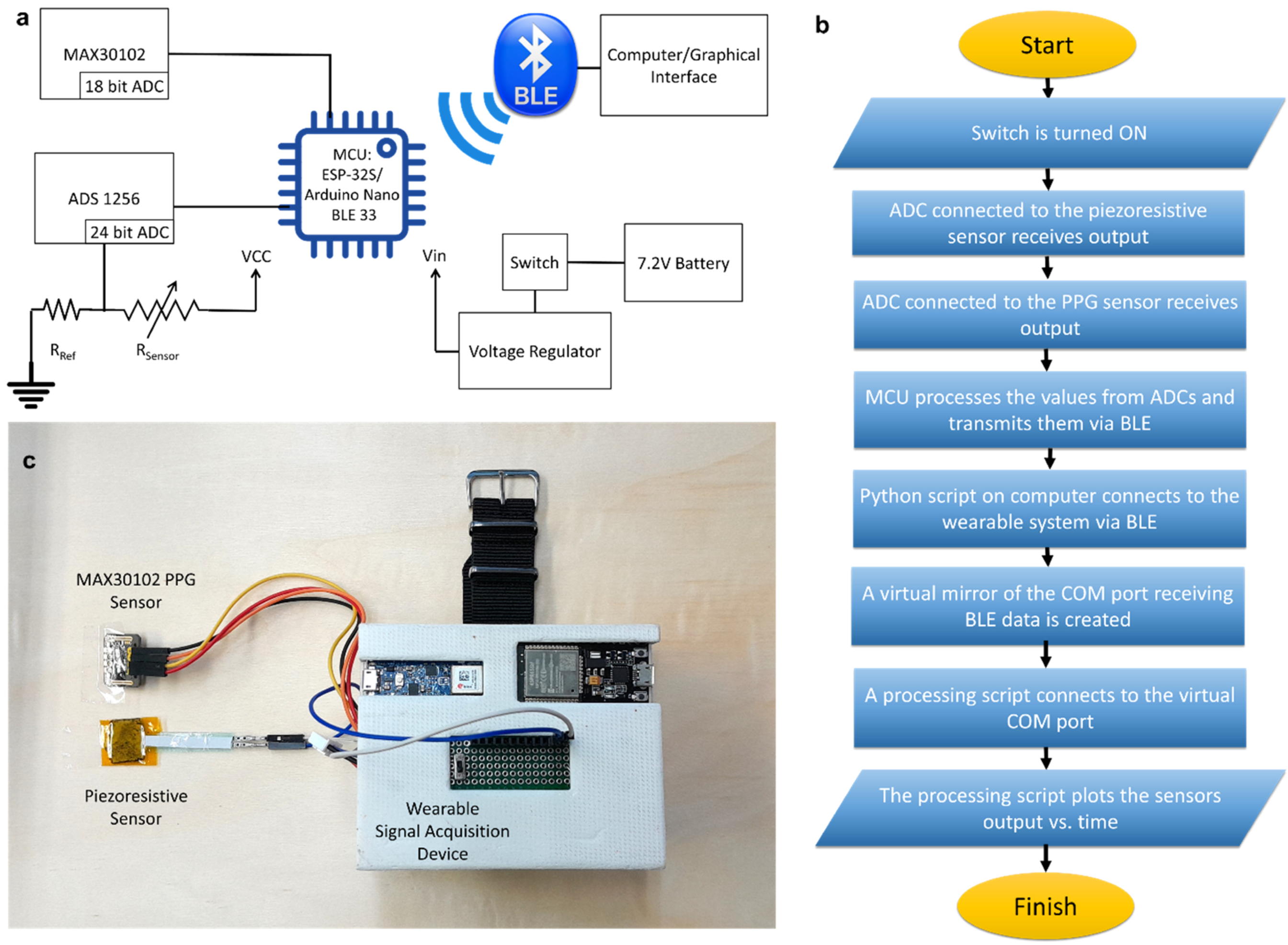

Figure 4. (a) Electrical schematic of different components of the wearable signal collection prototype. (b) Flowchart illustrating the process chain from signal acquisition to displaying the pulse waveform using the wearable signal collection prototype. (c) Signal collection prototype with PPG and dual piezoresistive sensors for simultaneous pulse waveform acquisition.

factors affecting the sensor's performance. Friction-induced heat generation between sensor layers as well as Joule heating may contribute to the increased resistance. Lastly, the apparatus itself, such as stepper motor overheating, could introduce minor inaccuracies in applied pressure, further affecting the sensor's output. Furthermore, the response time is an equally significant parameter when it comes to measuring a precisely timed occurrence such as cardiac activity. With its optimized design, the sensor boasts a rapid response and recovery time of 95 and 145 ms, respectively, at a loading of 10.1 kPa (see Figure 3d). The sensor exhibits a reliable sensing response during stepwise pressure increases from 9.25 to 86 kPa, as depicted in Figure 3e. Furthermore, the sensor demonstrates excellent performance when subjected to simulated heartbeats with a pressure amplitude of 15.3 kPa, corresponding to typical human systolic blood pressure. To simulate various physiological conditions, the frequency of these heartbeats was varied from 0.5 to 1 and 1.5 Hz, representing heart rates of 30, 60, and 90 beats per minute (BPM), respectively. These frequencies were chosen to mimic different activity levels: resting, normal daily activities, and exercise, as shown in Figure 3f. This testing highlights the sensor's ability to reliably detect pulse waveforms across a range of real-world conditions. Its properties, including high sensitivity, a broad pressure sensing range, and short response time, underscore the dual piezoresistive pressure sensor's significant potential for various practical applications, particularly pulse waveform detection. Our results suggest that the dual piezoresistive configuration offers an innovative approach to sensor assembly, providing a novel complementary solution for enhancing pressure sensor performance.

3.4. Data Collection and Processing. Despite advancements in wearable medical devices, achieving continuous monitoring of weak physiological signals during routine activities and physical exercise remains challenging. This difficulty arises from the need for complex signal processing circuitry, typically found in benchtop equipment like sourcemeters. Such equipment tends to be bulky and requires plug-in power, making it unsuitable for mobile use. Moreover, piezoresistive pressure sensors, commonly used in wearable devices, are prone to interference from body movements, which can compromise signal fidelity.

All of these factors together contribute to the ongoing challenge of developing reliable and practical mobile wearables for long-term and continuous physiological monitoring. The development of such a wearable signal acquisition device—high resolution, compact, and battery-powered—has been historically challenging. Advancement of versatile and open-sourced development boards (such as Arduino, ESP32, etc.) as well as efficient analog-to-digital converters (such as the

https://doi.org/10.1021/acsami.4c17710
ACS Appl. Mater. Interfaces 2024, 16, 65402−65413

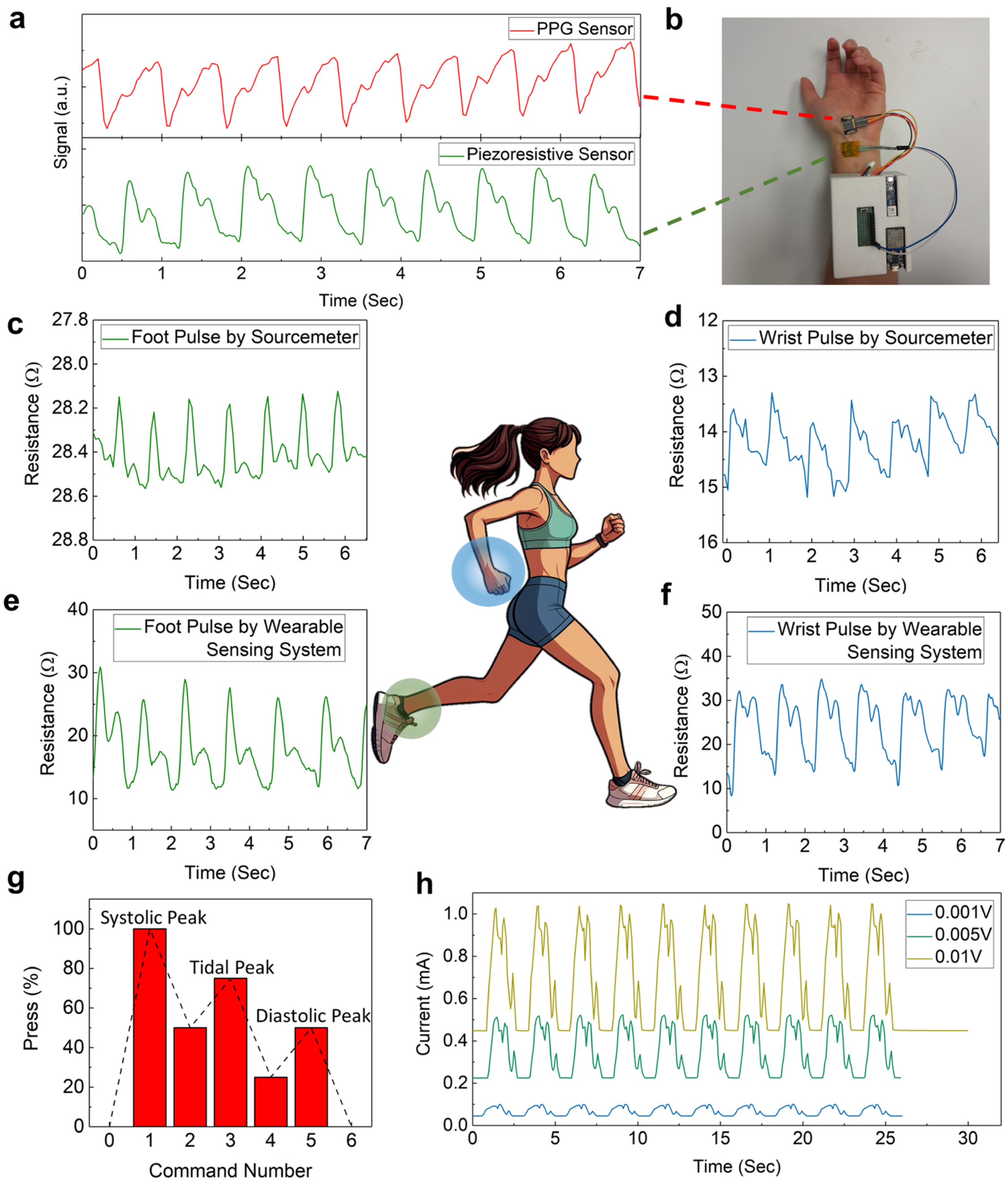

Figure 5. Practical application of the dual piezoresistive sensing system. (a) Simultaneous pulse waveform readout from the wrist using the dual piezoresistive pressure sensor and a PPG sensor. (b) Placement of the sensors when plot a was produced. (c) Ankle pulse produced by sourcemeter Keithley 2460 and (e) by the wearable sensing system. (d) Wrist pulse obtained by sourcemeter Keithley 2460 and (f) by the wearable sensing system. (g) Excitation signal produced by testbed to simulate a pulse waveform. (h) Dependency of the signal acquisition capability on the sourced voltage to capture the details of the pulse waveform from a shared excitation signal.

ADS1256 24-bit converter) enabled us to create a wearable signal acquisition prototype in this study. Our dual piezoresistive sensor offers promise due to its high sensitivity and linear relationship to the relevant pressure range of blood pressure (0−16 kPa), enabling the detection of subtle changes even in high-pressure regimes. When paired with a high-resolution signal acquisition device, the system can capture and display weak human physiological signals such as pulse waveforms from various body peripherals (wrist, ankle, etc.).

Powered by a 1000 mAh 7.2 V battery, this prototype (Figures 4a,c and S11) weighs 217 g and is capable of transmitting pulse waveform data in real-time to a computer for over 6 h on a single charge, achieving a maximum data resolution of 30 kHz. In this sensing system, a photoplethysmography (PPG) sensor is also integrated in order to provide added verification of the received signal, to effectively reject spikes caused by motion artifacts that may occur in one sensor but not the other. Figure 4b illustrates the operational steps from signal acquisition to display the pulse waveform on a computer or personal electronic device. This prototype employs Bluetooth low energy (BLE) for signal transmission once high-resolution digital signals from both the PPG and dual piezoresistive pressure sensor have been generated. In addition, the BLE offers a more energy-efficient mode of data

https://doi.org/10.1021/acsami.4c17710
ACS Appl. Mater. Interfaces 2024, 16, 65402−65413

transfer compared to classic Bluetooth protocols, making it ideal for this wearable system. Furthermore, tasks such as real-time plotting and potential data analysis are performed on a computer or personal electronic device, conserving battery power for signal acquisition rather than power-intensive tasks like data display. This approach optimizes energy usage and enhances the practicality of the wearable monitoring system for prolonged tests.

3.5. Dual Piezoresistive Pressure Sensor for Pulse Wave Monitoring. The pulse waveform stands out as one of the most crucial noninvasive cardiac vital signs. Beyond its applications in fitness tracking using peripheral body sensors, it holds immense potential for diagnosing and preventing not only cardiovascular diseases but also arterial peripheral diseases, which could serve as early indicators of conditions like diabetes.[38] The sustained sensitivity of the dual piezoresistive sensor across the blood pressure range (0−20 kPa) makes it well-suited for detecting such weak physiological signals. Thus, we explored the potential of our sensing system (comprising sensor and signal acquisition) for wearable pulse waveform detection by affixing the sensor to both the wrist and ankle areas (Figure 5). In Figure 5a,b, two sensors (dual piezoresistive and PPG sensors) were simultaneously placed on the wrist to capture pulse waveforms. As illustrated in Figure 5a, the sensor accurately records the body's pulse signals, with the typical peaks—percussion (P), tidal (T), and diastolic (D)—clearly discernible. This capability holds promise for enhancing the monitoring and diagnosis of cardiovascular and peripheral vascular conditions using wearable technology. Notably, the pulse waveform from the PPG sensor appears inverted compared to that from the dual piezoresistive sensor. This discrepancy arises from the sensors being positioned over different veins (see Figure S9), with one capturing the forward-going pulse wave and the other capturing the backward-going wave. Similar inverted pulse waveforms were also observed in this previous study[42] (see Video S1 for pulse detection on the same vein). Moreover, the integration of the PPG sensor enhances the robustness and versatility of the system. First, it allows for cross-validation of signals, improving accuracy by comparing data from two distinct sensing mechanisms: pressure and optical. Second, the dual-sensor setup ensures a robust performance under varied environmental conditions. The PPG sensor maintains reliability even when external forces or movement impact the piezoresistive sensor. Conversely, the dual piezoresistive sensor remains reliable, while the PPG sensor is adversely affected by ambient light, such as infrared (IR) radiation (Video S3). Finally, this integration facilitates the assessment of vascular stiffness, enabling simultaneous measurement of blood volume (PPG) and pressure waveforms (piezoresistive), which provides insights into vascular health and pulse wave velocity—a key metric in diagnosing cardiovascular conditions such as hypertension and arterial stiffness. Simultaneous detection of both phenomena could offer valuable insights into localized vascular health, facilitating the detection of conditions, such as arterial stenosis and venous insufficiency.

Figures 5c−f presents the wrist and foot (ankle) pulse waveforms acquired by the sourcemeter and the wearable sensing system, respectively (see Video S2). The waveforms are expressed as resistance change over time, with the sourcemeter readings obtained using the 4-wire method and the wearable sensing system readings calculated using a voltage divider circuit (see details in the Supporting Information). Notably, the wearable sensing system successfully captures the three characteristic features of the pulse waveform—systolic, diastolic notch, and diastolic peak—demonstrating a strong correlation with the signal obtained using the benchtop sourcemeter. These results confirm that the wearable system can accurately resolve key features of both ankle and wrist pulse waveforms, matching the performance of the sourcemeter.

This congruence underscores the reliability and accuracy of the wearable sensing system in capturing pulse waveforms, affirming its potential for practical applications in cardiovascular monitoring and diagnosis. Figure 5g illustrates the commands used to generate the simulated mechanical pulse waveform from our custom-made testbed. This mechanical excitation is designed to simulate a human pulse signal and serve as the input for testing the resolution power of our sensor system. Figure 5h, in turn, displays the current output of the sensor when subjected to this excitation signal under different sourced voltages (0.001, 0.005, and 0.01 V). The experiment demonstrates that the sensor's ability to capture the full details of the excitation signal depends on the sourced voltage. At a low sourced voltage (0.001 V), the sensor is unable to fully resolve the excitation waveform, as evidenced by a significant deviation from the mechanical pulse signal shown in Figure 5g. In particular, the systolic peak of the pulse is poorly represented, appearing significantly shorter than the Tidal peak. As the sourced voltage increases to 0.005 V, the sensor's output improves, capturing a waveform much closer to the input signal. At 0.01 V, the sensor output shows further amplification of the waveform, although the overall resolution of the waveform does not improve substantially. We observe this because the system's data point generation rate (resolution) remains fixed, so increasing the sourced voltage leads to higher current change (ΔI), which allows for better signal detection within the system's resolution limits. Beyond a certain voltage threshold, however, further increases do not significantly improve the signal's readout. This experiment underscores the importance of selecting an appropriate sourced voltage to optimize the sensor's performance in pulse waveform detection applications. Sourcing insufficient voltage leads to signal loss, while excessive voltage offers no further benefit once the system's resolution limit is reached.

The dual piezoresistive sensors show promising sensing performance suitable for continuous monitoring of pulse waveforms. This work has offered a fresh perspective on addressing the trade-off between sensitivity and linearity in piezoresistive pressure sensors. It should be noted that our wearable prototype allows for flexible sensor placement, strategically positioning the PPG sensor on veins near extremities, and can yield valuable insights into vascular health, including conditions such as arterial stenosis and venous insufficiency. Furthermore, by using PPG with a different mode of signal detection than the dual piezoresistive pressure sensor, the system can address specific noise issues associated with each type of sensor. For instance, the piezoresistive mode of detection may be prone to noise from temperature variations due to joule heating, power supply fluctuations, external electromagnetic interference, and mechanical vibrations. Conversely, PPG sensors can encounter noise issues caused by ambient light fluctuations, skin moisture affecting light scattering, and variations in skin pigmentation and thickness, all of which can distort the signal (refer to Video S3, which includes a video from our own experimentation

https://doi.org/10.1021/acsami.4c17710
ACS Appl. Mater. Interfaces 2024, 16, 65402−65413

demonstrating the noise induced by proximity to IR radiation). By leveraging complementary sensor technologies, the performance of this platform holds significant promise for enhancing the monitoring capabilities of wearable medical devices, paving the way for improved healthcare monitoring during daily activities and physical exertion.

4. CONCLUSIONS

In summary, this study shows the promising design of a dual piezoresistive sensor. The sensor is based on both micro-pyramid (for high sensitivity) and porous carbon grease-coated filter paper (for extending the range and linearity) as sensing layers. The synergy between these sensing components and the interdigitated electrode of the dual piezoresistive pressure sensor prevents signal saturation while exhibiting a high sensitivity value (8.2 kPa^{-1}). Moreover, this sensor displays robust durability, as it has been tested through 5000 cycles of synthetic two-staged waveforms. Furthermore, it retains the ability to capture intricate details of the pulse waveform, even after extended periods of operation. The short response time of 95/145 ms loading/unloading (at an applied pressure of 10.1 kPa) confirms that the sensor can operate efficiently in dynamic pressure sensing applications such as wrist-worn full pulse waveform acquisition. Integrating with the dual piezoresistive pressure sensors, we constructed a prototype wearable system with high-resolution, compact, and wearable signal acquisition capability. This system stands in contrast in size to conventional benchtop and complex sourcemeters which are typically necessary for low signal-to-noise ratio signals. Comparison of the results obtained from fully wearable pulse waveforms detection with conventional methods shows that our wearable system is capable of capturing all the details of the pulse waveforms on both wrist and ankle. Moreover, the versatility of the sensing system in this study allows a real-time comparison of the pulse waveform obtained from the dual piezoresistive sensor with state-of-the-art PPG sensors. This capability opens avenues for localized vascular monitoring (e.g., monitoring for vascular stenosis) enhancing the potential for advanced healthcare applications.

■ ASSOCIATED CONTENT

Supporting Information

The Supporting Information is available free of charge at https://pubs.acs.org/doi/10.1021/acsami.4c17710.

Simulation method, resistance change conversion in pulse waveform acquisition experiment, pulse waveform acquisition in the literature, piezoresistive sensor micro-fabrication method, interdigitated electrode dimensions, 3D simulation of piezoresistive sensor compression, dependency of signal detection capability on the sourced voltage, SEM view of porous piezoresistive sensor, mechanical testbed and its operational steps, hand's vein anatomy schematic, porous piezoresistive sensor fabrication method, internal components of the wearable sensing system, and table summarizing the state-of-the-art piezoresistive pressure sensors (PDF)

Video S1. Simultaneous pulse waveform detection using PPG and dual piezoresistive sensor (MP4)

Video S2. Pulse waveform acquisition from the foot acquisition (MP4)

Video S3. PPG sensor susceptibility to IR radiation (MOV)

■ AUTHOR INFORMATION

Corresponding Author

Chunlei Wang – *Department of Mechanical and Materials Engineering, Florida International University, Miami, Florida 33174, United States; Department of Mechanical and Aerospace Engineering, University of Miami, Coral Gables, Florida 33146, United States;* orcid.org/0000-0003-2574-7314; Email: wangc@miami.edu

Authors

Borzooye Jafarizadeh – *Department of Mechanical and Materials Engineering, Florida International University, Miami, Florida 33174, United States;* orcid.org/0000-0002-1790-9179

Azmal Huda Chowdhury – *Department of Mechanical and Materials Engineering, Florida International University, Miami, Florida 33174, United States;* orcid.org/0000-0003-0290-628X

Md Shariful Islam Sozal – *Department of Mechanical and Materials Engineering, Florida International University, Miami, Florida 33174, United States*

Zhe Cheng – *Department of Mechanical and Materials Engineering, Florida International University, Miami, Florida 33174, United States*

Nezih Pala – *Department of Electrical and Computer Engineering, Florida International University, Miami, Florida 33174, United States*

Complete contact information is available at: https://pubs.acs.org/10.1021/acsami.4c17710

Notes

The authors declare no competing financial interest.

■ ACKNOWLEDGMENTS

This work was partially supported by NSF awards 2423124 and 2412500. The authors would like to acknowledge the funding support from NSF award 1648451-Precise Advanced Technologies and Health Systems for Underserved Population Engineering Research Center (PATHS-UP ERC). B.J. and A.H.C. would like to acknowledge support from Dissertation Year Fellowship (DYF) and B.J. would like to acknowledge Doctoral Evidence Acquisition (DEA) Fellowship award from Florida International University Graduate School.

■ REFERENCES

(1) Chen, Z.; Qu, C.; Yao, J.; Zhang, Y.; Xu, Y. Two-Stage Micropyramids Enhanced Flexible Piezoresistive Sensor for Health Monitoring and Human-Computer Interaction. *ACS Appl. Mater. Interfaces* **2024**, *16* (6), 7640–7649.

(2) Zang, Y.; Zhang, F.; Di, C.; Zhu, D. Advances of Flexible Pressure Sensors toward Artificial Intelligence and Health Care Applications. *Mater. Horiz.* **2015**, *2* (2), 140–156.

(3) Li, M.; Liang, J.; Wang, X.; Zhang, M. Ultra-Sensitive Flexible Pressure Sensor Based on Microstructured Electrode. *Sensors* **2020**, *20* (2), 371.

(4) Kim, S. W.; Lee, J. H.; Ko, H. J.; Lee, S.; Bae, G. Y.; Kim, D.; Lee, G.; Lee, S. G.; Cho, K. Mechanically Robust and Linearly Sensitive Soft Piezoresistive Pressure Sensor for a Wearable Human-Robot Interaction System. *ACS Nano* **2024**, *18* (4), 3151–3160.

(5) Zhang, X.; Lu, L.; Wang, W.; Zhao, N.; He, P.; Liu, J.; Yang, B. Flexible Pressure Sensors with Combined Spraying and Self-Diffusion of Carbon Nanotubes. *ACS Appl. Mater. Interfaces* **2022**, *14* (33), 38409–38420.

https://doi.org/10.1021/acsami.4c17710
ACS Appl. Mater. Interfaces 2024, 16, 65402–65413

(6) Wang, J.; Suzuki, R.; Shao, M.; Gillot, F.; Shiratori, S. Capacitive Pressure Sensor with Wide-Range, Bendable, and High Sensitivity Based on the Bionic Komochi Konbu Structure and Cu/Ni Nanofiber Network. *ACS Appl. Mater. Interfaces* **2019**, *11* (12), 11928−11935.
(7) Garland, N. T.; Kaveti, R.; Bandodkar, A. J. Biofluid-Activated Biofuel Cells, Batteries, and Supercapacitors: A Comprehensive Review. *Adv. Mater.* **2023**, *35* (52), No. 2303197.
(8) Li, Y.; Lei, X.; Guo, D.; Zhao, Y.; Zeng, Z.; Yi, L.; Li, P.; Liu, F.; Ren, T. L. Laser-Induced Skin-like Flexible Pressure Sensor for Artificial Intelligence Speech Recognition. *ACS Appl. Mater. Interfaces* **2024**, *16* (8), 10380−10388.
(9) Yan, J.; Ma, Y.; Jia, G.; Zhao, S.; Yue, Y.; Cheng, F.; Zhang, C.; Cao, M.; Xiong, Y.; Shen, P.; Gao, Y. Bionic MXene Based Hybrid Film Design for an Ultrasensitive Piezoresistive Pressure Sensor. *Chem. Eng. J.* **2022**, *431*, No. 133458.
(10) Chowdhury, A. H.; Jafarizadeh, B.; Pala, N.; Wang, C. Paper-Based Supercapacitive Pressure Sensor for Wrist Arterial Pulse Waveform Monitoring. *ACS Appl. Mater. Interfaces* **2023**, *15*, 53043−53052.
(11) Chen, M.; Li, K.; Cheng, G.; He, K.; Li, W.; Zhang, D.; Li, W.; Feng, Y.; Wei, L.; Li, W.; Zhong, G.; Yang, C. Touchpoint-Tailored Ultrasensitive Piezoresistive Pressure Sensors with a Broad Dynamic Response Range and Low Detection Limit. *ACS Appl. Mater. Interfaces* **2019**, *11* (2), 2551−2558.
(12) Min, S.; Kim, D. H.; Joe, D. J.; Kim, B. W.; Jung, Y. H.; Lee, J. H.; Lee, B. Y.; Doh, I.; An, J.; Youn, Y. N.; Joung, B.; Yoo, C. D.; Ahn, H. S.; Lee, K. J. Clinical Validation of a Wearable Piezoelectric Blood-Pressure Sensor for Continuous Health Monitoring. *Adv. Mater.* **2023**, *35* (26), No. 2301627.
(13) Fang, Y.; Zou, Y.; Xu, J.; Chen, G.; Zhou, Y.; Deng, W.; Zhao, X.; Roustaei, M.; Hsiai, T. K.; Chen, J. Ambulatory Cardiovascular Monitoring Via a Machine-Learning-Assisted Textile Triboelectric Sensor. *Adv. Mater.* **2021**, *33* (41), No. e2104178.
(14) Shin, Y. E.; Sohn, S. D.; Han, H.; Park, Y.; Shin, H. J.; Ko, H. Self-Powered Triboelectric/Pyroelectric Multimodal Sensors with Enhanced Performances and Decoupled Multiple Stimuli. *Nano Energy* **2020**, *72*, No. 104671.
(15) Lee, Y.; Myoung, J.; Cho, S.; Park, J.; Kim, J.; Lee, H.; Lee, Y.; Lee, S.; Baig, C.; Ko, H. Bioinspired Gradient Conductivity and Stiffness for Ultrasensitive Electronic Skins. *ACS Nano* **2021**, *15* (1), 1795−1804.
(16) Li, W.; Jin, X.; Han, X.; Li, Y.; Wang, W.; Lin, T.; Zhu, Z. Synergy of Porous Structure and Microstructure in Piezoresistive Material for High-Performance and Flexible Pressure Sensors. *ACS Appl. Mater. Interfaces* **2021**, *13* (16), 19211−19220.
(17) Jafarizadeh, B.; Chowdhury, A. H.; Khakpour, I.; Pala, N.; Wang, C. Design Rules for a Wearable Micro-Fabricated Piezo-Resistive Pressure Sensor. *Micromachines* **2022**, *13* (6), 838.
(18) Liu, Y.; Xu, H.; Dong, M.; Han, R.; Tao, J.; Bao, R.; Pan, C. Highly Sensitive Wearable Pressure Sensor Over a Wide Sensing Range Enabled by the Skin Surface-Like 3D Patterned Interwoven Structure. *Adv. Mater. Technol.* **2022**, *7* (12), No. 2200504.
(19) Cheng, Y.; Ma, Y.; Li, L.; Zhu, M.; Yue, Y.; Liu, W.; Wang, L.; Jia, S.; Li, C.; Qi, T.; Wang, J.; Gao, Y. Bioinspired Microspines for a High-Performance Spray Ti3C2Tx MXene-Based Piezoresistive Sensor. *ACS Nano* **2020**, *14* (2), 2145−2155.
(20) Kim, Y. R.; Kim, M. P.; Park, J.; Lee, Y.; Ghosh, S. K.; Kim, J.; Kang, D.; Ko, H. Binary Spiky/Spherical Nanoparticle Films with Hierarchical Micro/Nanostructures for High-Performance Flexible Pressure Sensors. *ACS Appl. Mater. Interfaces* **2020**, *12* (52), 58403−58411.
(21) Gao, L.; Zhu, C.; Li, L.; Zhang, C.; Liu, J.; Yu, H. D.; Huang, W. All Paper-Based Flexible and Wearable Piezoresistive Pressure Sensor. *ACS Appl. Mater. Interfaces* **2019**, *11* (28), 25034−25042.
(22) Li, H.; Wu, K.; Xu, Z.; Wang, Z.; Meng, Y.; Li, L. Ultrahigh-Sensitivity Piezoresistive Pressure Sensors for Detection of Tiny Pressure. *ACS Appl. Mater. Interfaces* **2018**, *10* (24), 20826−20834.
(23) Luo, N.; Dai, W.; Li, C.; Zhou, Z.; Lu, L.; Poon, C. C. Y.; Chen, S. C.; Zhang, Y.; Zhao, N. Flexible Piezoresistive Sensor Patch Enabling Ultralow Power Cuffless Blood Pressure Measurement. *Adv. Funct Mater.* **2016**, *26* (8), 1178−1187.
(24) Yang, G.; Yang, Y.; Chen, T.; Wang, J.; Ma, L.; Yang, S. Graphene/MXene Composite Aerogels Reinforced by Polyimide for Pressure Sensing. *ACS Appl. Nano Mater.* **2022**, *5* (1), 1068−1077.
(25) Yu, Z.; Xu, J.; Gong, H.; Li, Y.; Li, L.; Wei, Q.; Tang, D. Bioinspired Self-Powered Piezoresistive Sensors for Simultaneous Monitoring of Human Health and Outdoor UV Light Intensity. *ACS Appl. Mater. Interfaces* **2022**, *14* (4), 5101−5111.
(26) Sun, Q. J.; Zhao, X. H.; Yeung, C. C.; Tian, Q.; Kong, K. W.; Wu, W.; Venkatesh, S.; Li, W. J.; Roy, V. A. L. Bioinspired, Self-Powered, and Highly Sensitive Electronic Skin for Sensing Static and Dynamic Pressures. *ACS Appl. Mater. Interfaces* **2020**, *12* (33), 37239−37247.
(27) Li, L.; Bao, X.; Meng, J.; Zhang, C.; Liu, T. Sponge-Hosting Polyaniline Array Microstructures for Piezoresistive Sensors with a Wide Detection Range and High Sensitivity. *ACS Appl. Mater. Interfaces* **2022**, *14* (26), 30228−30235.
(28) Huang, J.; Zeng, J.; Liang, B.; Wu, J.; Li, T.; Li, Q.; Feng, F.; Feng, Q.; Rood, M. J.; Yan, Z. Multi-Arch-Structured All-Carbon Aerogels with Superelasticity and High Fatigue Resistance as Wearable Sensors. *ACS Appl. Mater. Interfaces* **2020**, *12* (14), 16822−16830.
(29) Choong, C.; Shim, M.; Lee, B.; S, J.-A.; et al. Highly Stretchable Resistive Pressure Sensors Using a Conductive Elastomeric Composite on a Micropyramid Array. *Adv. Mater.* **2014**, *26* (21), 3451−3458.
(30) Wang, X.; Gu, Y.; Xiong, Z.; Cui, Z.; Zhang, T. Silk-Molded Flexible, Ultrasensitive, and Highly Stable Electronic Skin for Monitoring Human Physiological Signals. *Adv. Mater.* **2014**, *26* (9), 1336−1342.
(31) Park, J.; Kim, M.; Lee, Y.; Lee, H.; Ko, H. Fingertip Skin− Inspired Microstructured Ferroelectric Skins Discriminate Static/ Dynamic Pressure and Temperature Stimuli. *Sci Adv.* **2015**, *30* (9), No. e1500661.
(32) Duan, S.; Yang, H.; Hong, J.; Li, Y.; Lin, Y.; Zhu, D.; Lei, W.; Wu, J. A Skin-beyond Tactile Sensor as Interfaces between the Prosthetics and Biological Systems. *Nano Energy* **2022**, *102*, No. 107665.
(33) Pei, Z.; Zhang, Q.; Yang, K.; Yuan, Z.; Zhang, W.; Sang, S. A Fully 3D-Printed Wearable Piezoresistive Strain and Tactile Sensing Array for Robot Hand. *Adv. Mater. Technol.* **2021**, *6* (7), No. 2100038.
(34) Zhao, T.; Yuan, L.; Li, T.; Chen, L.; Li, X.; Zhang, J. Pollen-Shaped Hierarchical Structure for Pressure Sensors with High Sensitivity in an Ultrabroad Linear Response Range. *ACS Appl. Mater. Interfaces* **2020**, *12* (49), 55362−55371.
(35) Guan, H.; Meng, J.; Cheng, Z.; Wang, X. Processing Natural Wood into a High-Performance Flexible Pressure Sensor. *ACS Appl. Mater. Interfaces* **2020**, *12* (41), 46357−46365.
(36) Wang, Y.; Chao, M.; Wan, P.; Zhang, L. A Wearable Breathable Pressure Sensor from Metal-Organic Framework Derived Nano-composites for Highly Sensitive Broad-Range Healthcare Monitoring. *Nano Energy* **2020**, *70*, No. 104560.
(37) Zhang, C.; Bin Ye, W.; Zhou, K.; Chen, H.-Y.; Yang, J.-Q.; Ding, G.; Chen, X.; Zhou, Y.; Zhou, L.; Li, F.; Han, S.-T.; Zhang, C.; Ye, W. B.; Zhou, K.; Yang, J.; Ding, G.; Chen, X.; Zhou, L.; Han, S.; Chen, H.; Zhou, Y.; Li, F. Bioinspired Artificial Sensory Nerve Based on Nafion Memristor. *Adv. Funct Mater.* **2019**, *29* (20), No. 1808783.
(38) Laurent, S.; Cockcroft, J.; Van Bortel, L.; Boutouyrie, P.; Giannattasio, C.; Hayoz, D.; Pannier, B.; Vlachopoulos, C.; Wilkinson, I.; Struijker-Boudier, H. Expert Consensus Document on Arterial Stiffness: Methodological Issues and Clinical Applications. *Eur. Heart J.* **2006**, *27* (21), 2588−2605.
(39) Zappielo, C. D.; Nanicuacua, D. M.; Dos Santos, W. N. L.; Da Silva, D. L. F.; Dall'antônia, L. H.; De Oliveira, F. M.; Clausen, D. N.; Tarley, C. R. T. Solid Phase Extraction to On-Line Preconcentrate Trace Cadmium Using Chemically Modified Nano-Carbon Black

https://doi.org/10.1021/acsami.4c17710
ACS Appl. Mater. Interfaces 2024, 16, 65402−65413

with 3-Mercaptopropyltrimethoxysilane. *J. Braz. Chem. Soc.* **2016**, *27* (10), 1715−1726.
(40) Stuart, B. H.Infrared Spectroscopy: Fundamentals and Applications. In *Infrared Spectroscopy: Fundamentals and Applications* 2004; pp 76−78 .
(41) Jafarizadeh, B.; Chowdhury, A. H.; Sozal, M. S. I.; Cheng, Z.; Pala, N.; Wang, C. Hardware and Protocol for Testing of Piezoresistive Pressure Sensors for Pulse Wave Monitoring. *IEEE Sens Lett.* **2023**, 7 (8), 1.
(42) Amelard, R.; Hughson, R. L.; Greaves, D. K.; Pfisterer, K. J.; Leung, J.; Clausi, D. A.; Wong, A. Non-Contact Hemodynamic Imaging Reveals the Jugular Venous Pulse Waveform. *Sci. Rep.* **2017**, 7 (1), No. 40150.

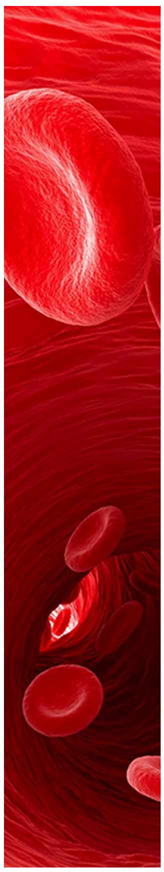

CAS BIOFINDER DISCOVERY PLATFORM™
CAS BIOFINDER HELPS YOU FIND YOUR NEXT BREAKTHROUGH FASTER
Navigate pathways, targets, and diseases with precision
Explore CAS BioFinder
CAS
A division of the American Chemical Society

https://doi.org/10.1021/acsami.4c17710
ACS Appl. Mater. Interfaces 2024, 16, 65402−65413